

## Two well-defined motifs in the cAMP-dependent protein kinase inhibitor (PKI $\alpha$ ) correlate with inhibitory and nuclear export function

JENNIFER A. HAUER,<sup>1</sup> PHILIPPE BARTHE,<sup>2</sup> SUSAN S. TAYLOR,<sup>1</sup>  
JOSEPH PARELLO,<sup>3</sup> AND ANDRÉ PADILLA<sup>2</sup>

<sup>1</sup>Department of Chemistry and Biochemistry, University of California, San Diego, 9500 Gilman Drive, La Jolla, California 92093-0654

<sup>2</sup>Centre de Biochimie Structurale CNRS UMR 9955, INSERM U414, University of Montpellier I, 15 Av. Charles Flahault, 34060 Montpellier Cedex 1, France

<sup>3</sup>UPRESA, 5-74 CNRS, University of Montpellier I, France, and Cancer Research Center, The Burnham Institute, 10901 N. Torrey Pines Rd., La Jolla, California 92037

(RECEIVED July 29, 1998; ACCEPTED November 30, 1998)

### Abstract

The heat stable inhibitor of cAMP-dependent protein kinase (PKI $\alpha$ ) contains both a nuclear export signal (NES) and a high affinity inhibitory region that is essential for inhibition of the catalytic subunit of the kinase. These functions are sequentially independent. Two-dimensional NMR spectroscopy was performed on uniformly [<sup>15</sup>N]-labeled PKI $\alpha$  to examine its structure free in solution. Seventy out of 75 residues were identified, and examination of the C $\alpha$ H chemical shifts revealed two regions of upfield chemical shifts characteristic of  $\alpha$ -helices. When PKI $\alpha$  was fragmented into two functionally distinct peptides for study at higher concentrations, no significant alterations in chemical shifts or secondary structure were observed. The first ordered region, identified in PKI $\alpha$  (1–25), contains an  $\alpha$ -helix from residues 1–13. This helix extends by one turn the helix observed in the crystal structure of a PKI $\alpha$  (5–24) peptide bound to the catalytic subunit. The second region of well-defined secondary structure, residues 35–47, overlaps with the nuclear export signal in the PKI $\alpha$  (26–75) fragment. This secondary structure consists of a helix with a hydrophobic face comprised of Leu37, Leu41, and Leu44, followed by a flexible turn containing Ile46. These four residues are critical for nuclear export function. The remainder of the protein in solution appears relatively unstructured, and this lack of structure surrounding a few essential and well-defined signaling elements may be characteristic of a growing family of small regulatory proteins that interact with protein kinases.

**Keywords:** 2D-NMR; cAPK; conformational disorder; kinase inhibitor; nuclear export signal; PKI $\alpha$

Signaling through cAMP-dependent protein kinase (cAPK) is a common pathway for many cellular processes. Regulation of cAPK is achieved by both inhibition and subcellular localization. The best understood control mechanism for cAPK kinase activity is

achieved through the regulatory (R) subunit. Two catalytic (C) subunits bind to a dimer of R subunits to yield an inactive holoenzyme. Cooperative binding of two molecules of cAMP to each R subunit causes dissociation of the holoenzyme complex and release of two active C subunits (Taylor et al., 1990). In addition to being inhibitors of C, the R subunits also contribute directly to subcellular localization of cAPK by interacting with A Kinase Anchoring Proteins (AKAPs). These proteins anchor the cAPK holoenzyme complex to a wide variety of cellular locations (Dell'Acqua & Scott, 1997).

Another mode by which cAPK is simultaneously localized and inhibited is by PKI, the heat stable protein kinase inhibitor identified by Walsh et al. (1971). While PKI $\alpha$  has only 75 residues, it has two sequentially distinct functional elements. The first third of PKI $\alpha$  contains the cAPK pseudo-substrate sequence preceded by a high affinity binding region. This segment contains nearly all of the residues critical for the subnanomolar inhibitory constant of

Reprint requests to: Susan S. Taylor, Department of Chemistry and Biochemistry, University of California, San Diego, 9500 Gilman Drive, La Jolla, California 92093-0654; e-mail: staylor@ucsd.edu.

**Abbreviations:** 1D, one-dimensional; 2D, two-dimensional; PKI $\alpha$ ,  $\alpha$  isoform of the heat-stable inhibitor of cAMP-dependent protein kinase; NES, nuclear export signal; D<sub>2</sub>O, <sup>2</sup>H<sub>2</sub>O; CD, circular dichroism; FTIR, Fourier transform infrared spectroscopy; NMR, nuclear magnetic resonance; HSQC, heteronuclear single quantum coherence spectroscopy; HMQC, heteronuclear multiple quantum coherence spectroscopy; COSY, correlation spectroscopy; NOESY, nuclear Overhauser effect spectroscopy; DQF-COSY, double quantum filtered correlation spectroscopy; NOE, nuclear Overhauser effect; CSI, chemical shift index; TPPI, time proportional phase incrementation; RMSD, root-mean-square deviation.

PKI $\alpha$  for the kinase (Walsh et al., 1971, 1990; Ashby & Walsh, 1973; Scott et al., 1985). A portion of this domain of PKI $\alpha$  (residues 5–24) was cocrystallized with the C subunit (Zheng et al., 1991), and the high affinity binding region was found to be  $\alpha$ -helical (Knighton et al., 1991a). A synthetic peptide corresponding to residues 5 to 22 of PKI $\alpha$  was also shown in solution to contain an  $\alpha$ -helix at its N-terminus by 1D NMR (Reed et al., 1989). In addition to inhibiting the kinase, PKI $\alpha$  also traffics the catalytic subunit from the nucleus to the cytoplasm through its Nuclear Export Signal (NES). The NES (residues 37–46) consists of a regular repeat of large hydrophobic amino acids, and acts to rapidly and actively export from the nucleus to the cytoplasm any protein to which it is bound, including the catalytic subunit in a C:PKI $\alpha$  complex (Fantozzi et al., 1994; Wen et al., 1995).

Based on CD and FTIR studies, PKI $\alpha$  does not appear to be highly structured in solution (Thomas et al., 1991). CD measurements indicated that PKI $\alpha$  has 21%  $\alpha$ -helix, 15% antiparallel  $\beta$ -sheet, 34% turn, and 30% random coil. This suggested the presence of another helix in PKI $\alpha$ , in addition to the N-terminal helix described previously.

Determining the structural features of PKI $\alpha$  is critical for understanding its bifunctionality. How does the structure of such a small protein allow for both high affinity binding to the C subunit and export of the enzyme complex from the nucleus? A structural study of the inhibitor free in solution was undertaken by 2D NMR to define structural features within the full length protein. Due to severe overlapping of proton resonances, uniformly  $^{15}\text{N}$  enriched PKI $\alpha$  was used to resolve most of the proton resonances as well as the proton–proton nuclear Overhauser effect (NOE) connectivities. Two regions of  $\alpha$ -helix were identified by Chemical Shift Index analysis, but overall there was a lack of medium- and long-range NOEs. This indicated that PKI $\alpha$  has a rather flexible structure in solution, and the presence of different shape “conformers” of PKI was apparent from early studies as well (Whitehouse & Walsh, 1982). At this point we adopted a strategy to analyze, by homonuclear 2D NMR, two functionally separate fragments, allowing the secondary structure of each functional domain to be more precisely determined. We identified two  $\alpha$ -helices, which overlap with the two functional elements of PKI $\alpha$ . The remainder of the molecule appears to be highly disordered.

## Results

### Sequential assignments of [ $^{15}\text{N}$ ]PKI $\alpha$

Figure 1 shows the HSQC spectrum of uniformly  $^{15}\text{N}$  labeled [Gly0]PKI $\alpha$ . As reported in Figure 2 and Table 1 of the Electronic Supplementary Material, 70 of 75 spin systems expected were sequentially assigned through a combination of HMQC-TOCSY and HMQC-NOESY spectra. Side-chain  $\text{C}\delta\text{H}_3$  resonances of Leu residues were assigned using NOE connectivities in the HMQC-NOESY spectra. One spin system has been tentatively assigned to Asp24 according to standard chemical shift values for aspartic acid (Wüthrich, 1986), and the most high-field shifted  $^{15}\text{N}$ -NH cross peak has been assigned to Arg15 by comparison with the [Gly0]PKI $\alpha$ (1–25) peptide spectra (see below).

No medium- or long-range NOEs were observed in the HMQC-NOESY spectra. This may be because the protein appears to be flexible in solution, with a relatively low content of secondary structure elements. This would reduce the NOE intensities through an equilibrium between relatively structured and less structured

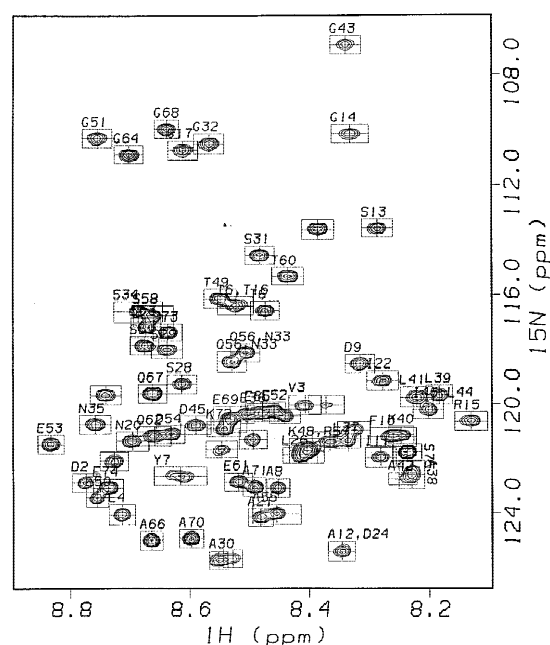


**Fig. 1.** Contour plot of the heteronuclear single quantum coherence spectrum of [ $^{15}\text{N}$ ] Gly0PKI $\alpha$  at pH 6.6 and 2 °C at 600 MHz. Cross peaks are labeled by residue number and one letter code.

states of the protein. Alternatively, analysis of PKI by dynamic light scattering at the concentration used for the NMR experiments showed that the inhibitor aggregates in solution (data not shown). The presence of such polymeric species could affect the NOE intensities through dynamic processes involving a variety of environments to given proton nuclei.

### Identification of secondary structure elements in PKI $\alpha$

To identify any regions of secondary structure within full length PKI $\alpha$ , the  $\text{CaH}$  chemical shift values in ppm of the 70 assigned residues were compared with the random coil chemical shift values for residues in a GGXGG peptide (Merutka et al., 1995), revealing two regions of upfield shifted  $\text{CaH}$  chemical shifts (Fig. 3). Chemical shift index analysis of these  $\text{CaH}$  chemical shift values identified these upfield shifted regions as helical. The first  $\alpha$ -helical region extends from residue 7 to 13, and corresponds to the high affinity binding helix seen in the crystal structure. Residues 2 and 3 also have indices of  $-1$ , suggesting an earlier start to the helix. The second helix identified is from residue 34 to 43 of PKI $\alpha$ , and overlaps with the Nuclear Export Signal of PKI $\alpha$ . The overall distribution of  $-1$  indices in this region is less than the previous helix, but two of the residues with “0” index values (35 and 42) differ from the tabulated  $\text{CaH}$  chemical shifts by  $-0.09$  ppm, indicating a consistent trend in upfield chemical shifts and these residues are indicated in Figure 3 by asterisks. These residues were included in defining the helix. Residue 44 has an index value of  $+1$ , terminating the helix. One other region of  $-1$  chemical shift indices is seen: a stretch of three  $-1$  values from 54 to 56. Three  $-1$  values are not enough to define an  $\alpha$ -helix, but suggest some secondary structure in this region. The remainder of PKI $\alpha$  is not structured.

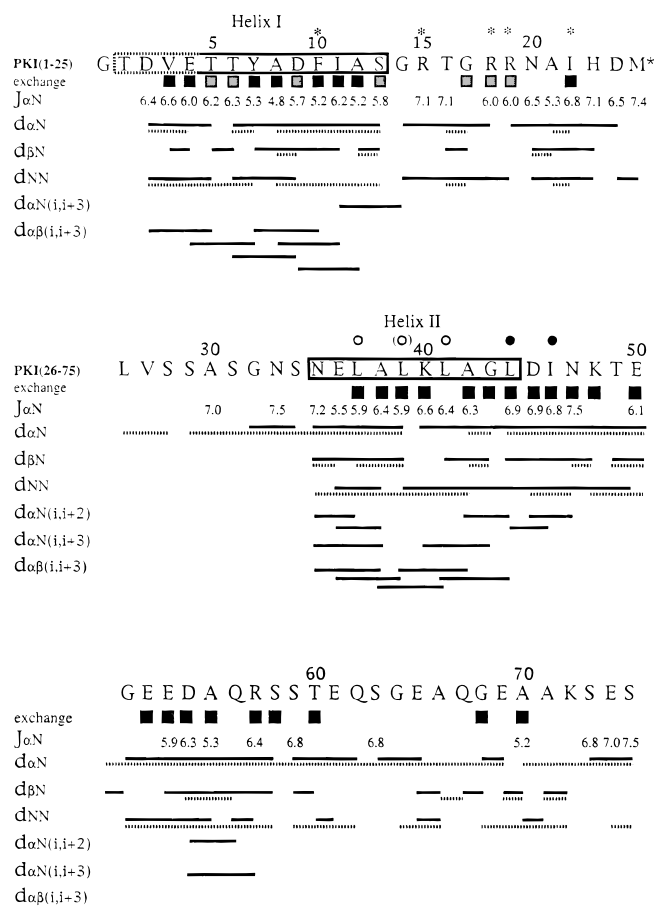


**Fig. 2.** Schematic overview of the sequential and medium range NOEs as inferred from the HMQC-NOESY spectrum of  $^{15}\text{N}$  labeled PKI (dashed lines) and from the NOESY spectra of the two PKI fragments (solid lines). For the fragments, slow exchanging amide protons, which gave cross peaks in the COSY in  $\text{D}_2\text{O}$ , are indicated by black squares, and for the N-terminal fragment (see Materials and methods) gray squares indicate cross peaks, which were absent in a second COSY spectrum in  $\text{D}_2\text{O}$ . Values of  $J_{\alpha\text{N}}$  coupling constants in bold were measured using the procedure of Ludvigsen et al. (1991). Other values are the line separation in the DQF-COSY spectra. The two helices are identified by the boxed residues with the helix cap indicated by dashed lines. \*, Residues critical for high affinity binding to cAPK; ●, residues essential for Nuclear Export Signal; ○, residues together essential for Nuclear Export Signal; ○, residue that does not play a role in Nuclear Export.

### Sequential assignments of PKI fragments

Based on the chemical shift index identification of the two helices but the lack of corresponding medium- and long-range NOEs to substantiate these helices in full length PKI, we decided to investigate the secondary structure of two functionally distinct PKI fragments, with the expectation that polydispersity in solution could be reduced, if not totally avoided.  $[\text{G}_0, \text{I}_{25}\text{M}] \text{PKI}\alpha$  was designed to allow two functional domains to be produced after cyanogen bromide cleavage. The resulting N-terminal fragment retains inhibitory capacity, while the C-terminal fragment possesses full nuclear export ability (data not shown).

Proton resonances of the two fragments of  $[\text{Gly}_0] \text{PKI}\alpha$  were assigned by the standard 2D-NMR strategy (Fig. 2, Table 1) (Wüthrich, 1986). For the N-terminal fragment, all sequential assignments were made, with the exception of the sequential con-

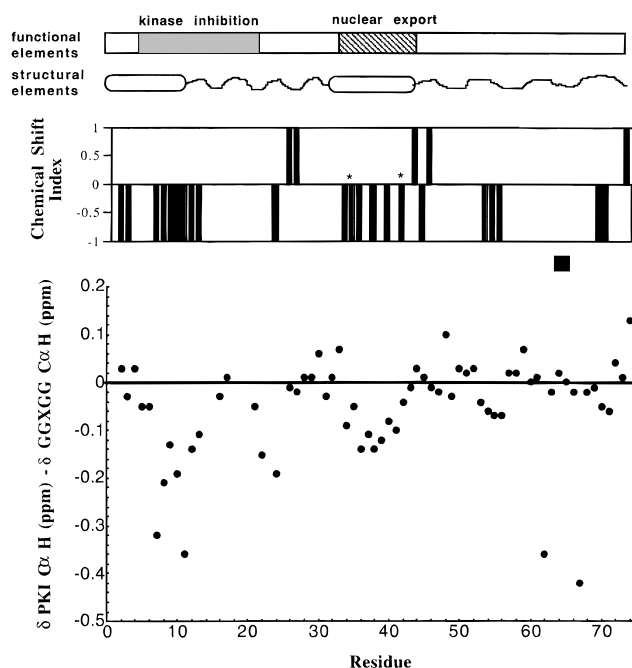


**Fig. 3.** Chemical Shift Index analysis of  $\text{C}\alpha\text{H}$  protons of  $^{15}\text{N}$  Gly $_0$  PKI $\alpha$  and deviation in the chemical shift of these same protons from random coil values. For the Chemical Shift Index analysis, each  $\text{C}\alpha\text{H}$  chemical shift was compared with tabulated values in Wishart et al. (1992). Deviations of  $\pm 0.1$  ppm were assigned values of  $\pm 1$ . The  $\text{C}\alpha\text{H}$  chemical shifts of two residues deviate by  $-0.09$ , and these are indicated with asterisks. Random coil values were obtained from Merutka et al. (1995). The locations of functional motifs and secondary structure are indicated above.

nectivity between Ser13 and Gly14. Due to the low solubility of the N-terminal fragment near neutral pH, all studies were performed at pH values close to 4. In the C-terminal fragment, all but five sequential  $d_{\alpha\text{N}}$  connectivities from Gly32 to Glu65 were assigned. This fragment has a high content of serine and glutamic acid residues, and several of their  $\text{NH}-\text{C}\alpha\text{H}$  cross peaks in the fingerprint region are superimposed. Three Ser residues, Ser28, Ser29, and Ser31, among nine in total, could not be identified. The residues Leu26 and Ala30 were assigned at the latest stage to the remaining spin systems. Despite strong overlap, several  $J_{\alpha\text{N}}$  coupling constants were measured.

### Comparison of chemical shifts

We compared the chemical shifts of full length PKI $\alpha$  and the PKI $\alpha$ (26–75) fragment to look for any conformational changes that may have occurred upon fragmentation. Five chemical shift differences could not be calculated due to the absence of proton resonance assignments in either full length or fragmented PKI $\alpha$ . As can be seen in Figure 4, chemical shift differences of both  $\text{NH}$  and  $\text{C}\alpha\text{H}$  are less than 0.05 ppm for most residues in PKI $\alpha$ (26–75). This indicates that no dramatic change occurs in the magnetic environment of the  $\text{NH}$  and  $\text{C}\alpha\text{H}$  protons, and therefore in the secondary and tertiary structure, upon fragmentation. No large changes are evident in the N-terminal fragment either, but this is less meaningful since the experiments were performed at quite different pH values. Any differences observed are likely to correspond to local conformational changes, since none of them involves several adjacent residues in the sequence.

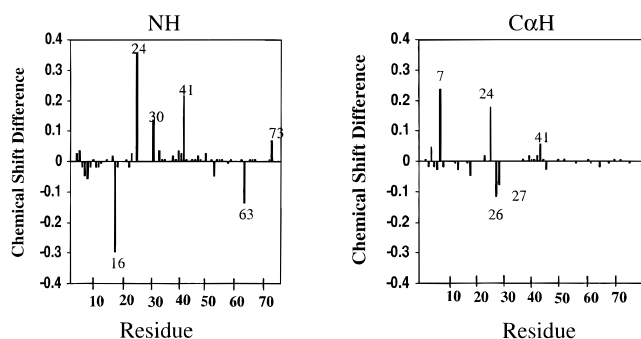


**Fig. 4.** The difference in NH and CαH chemical shifts between full length PKIα and the fragments.

#### Secondary structure of PKI fragments

α-Helices are characterized by sets of ( $i, i + 3$ ) NOE connectivities, slow NH exchange rates, and  $J_{\alpha N}$  coupling constants less than or equal to 6 Hz. By such criteria, two helices were identified in the fragments of PKIα, corresponding to the regions of α-helix identified by the Chemical Shift Index. Helix I extends from Asp2 to Ser13 of [Gly0]PKIα(1–25) and Helix II from Asn35 to Leu44 of PKIα(26–75). Molecular models of each of the two α-helical regions were constructed from the distance constraints imposed by the NOEs. Superimposition of the family of structures generated for the backbone stretch of Thr1–Ser13 gave an average rmsd value of 1.11 Å (Fig. 5) and ensemble-averaged refinement was applied to the average structure.

The N-terminus of PKIα (Thr-Asp-Val-Glu) appears to act as an N-capping motif. In such a motif, the first and fourth residues of a helix make two additional intrahelical hydrogen bonds, but depart from the helical values for  $\Phi$  and  $\Psi$  angles (Presta & Rose, 1988; Richardson & Richardson, 1988). Slow NH exchange rates were observed for Val3 and Glu4, and we found a NOE between  $C\gamma H_3$ Thr1 and NH Val3, in agreement with the geometrical requirements of an N-capping sequence (Zhou et al., 1994). Some variability does occur in the N-terminal stretch as shown by ensemble-averaged refinement and the  $B$ -factors for these first four residues are higher than for the rest of the helix (Fig. 6). We conclude overall that the first helix starts with the N-capping sequence from Thr1 to Glu4, a highly conserved sequence in all PKI isoforms identified. A small  $J_{\alpha N}$  value and a slow NH exchange rate for Ser13, in contrast to a fast NH exchange for Gly14, indicates that Ser13 is the last residue in Helix I.

A second helix (Helix II) was found within the C-terminal fragment, from Asn35 to Leu44, defined by a set of  $d\alpha N(i, i + 3)$  and  $d\alpha\beta(i, i + 3)$  NOE connectivities (Fig. 2). This helix, following ensemble-averaged refinement applied to the average structure, is

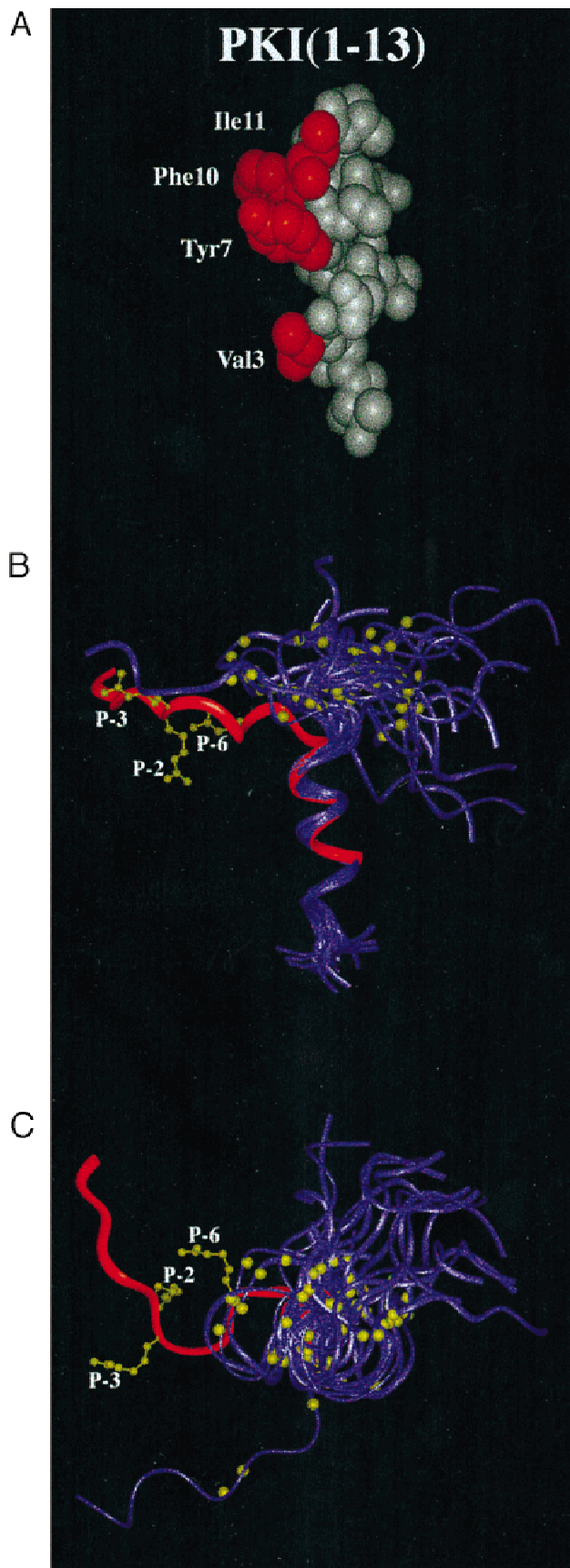


**Fig. 5.** A: Space filling model of PKIα(1–13). The hydrophobic residues critical for high affinity binding are labeled and shown in red. B: Superimposition of 23 structures for PKIα(1–25) from the NMR data in purple and PKIα(5–24) from the crystal structure in red (1APM) (Knighton et al., 1991b). The location of the three Arg residues is highlighted in each structure and the position of the residues is indicated in the PKIα(5–24) structure. C: A 90° rotation of the view in B with the three Arg residues highlighted in each peptide.

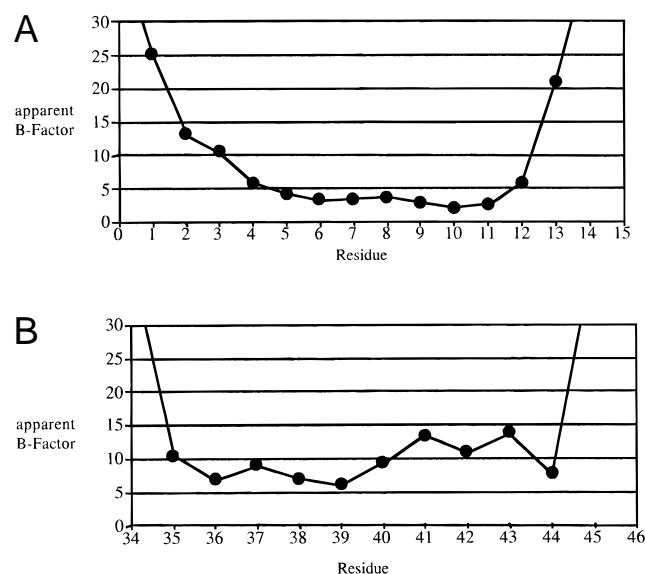


**Fig. 6.** Backbone residue  $B$ -factors of (A) Helix I in [Gly0]PKI $\alpha$ (1–25) and (B) Helix II in PKI $\alpha$ (26–75) from the NMR structures obtained with ensemble-averaged distance restraints. The effective  $B$ -factors were calculated from the RMSD ( $u$ ) from the average position using  $B = 8/3(\pi^2 u^2)$ .

displayed in Figure 7. The average RMSD value for the superimposition of this backbone stretch was 1.30 Å. In contrast to Helix I, this helix displays several  $J\alpha N$  constants that are slightly greater than 6 Hz, ranging from 6.3 to 6.6 Hz. Two large  $J\alpha N$  coupling constant values, 7.4 and 6.3 Hz, were found at the N- and

C-terminal residues of the helix, Asn35 and Leu44. This is not surprising since the ends of a helix are expected to “fray” due to weak individual H-bonds. Ensemble-averaged refinement indicates relatively low  $B$ -factors (between 5–10 Å<sup>2</sup>) for the stretch of residues between 35 and 40, whereas higher  $B$ -factors are found for the C-terminal half of this helix (Fig. 6). Several NOE connectivities of type ( $i, i + 2$ ) are found at the C-terminus of Helix II, between Gly43 and Asp45, Leu44 and Ile46, and Asp45 and Asn47. This is consistent with Helix II having a well-defined N-terminal half whereas the C-terminal half is much more flexible. The last observed NOE connectivity of type ( $i, i + 3$ ) indicates the break in Helix II occurs at Leu44. Interestingly, Asp45, Ile46, Asn47, and Lys48 have slow NH exchange rates, which indicates protection from solvent accessibility. Residues 44 to 47, while not participating in Helix II, certainly do not adopt a random conformation, but rather can be better described as a flexible turn structure.

Both helices have amphipathic character with one face of the helix formed by hydrophobic residues: Val3, Tyr7, Phe10, and Ile11 for Helix I (Fig. 5A), and Leu37, Ala38, Leu41, Ala42, and Leu44 for Helix II (Fig. 7). Helix I starts with an N-cap motif, which is less constrained than the core of the helix. In Helix II, the essential leucine residues cluster along the hydrophobic face of the helix, including Leu37, Leu41, and Leu44. Leu39, which does not play a role in the NES, lies on the opposite face. Two polar residues, Glu36 and Lys40, are found on the polar face of Helix II where they may form an ionic interaction.

## Discussion

Free PKI $\alpha$  in solution has two  $\alpha$ -helical regions surrounded by stretches of unstructured residues, and each helix overlaps with

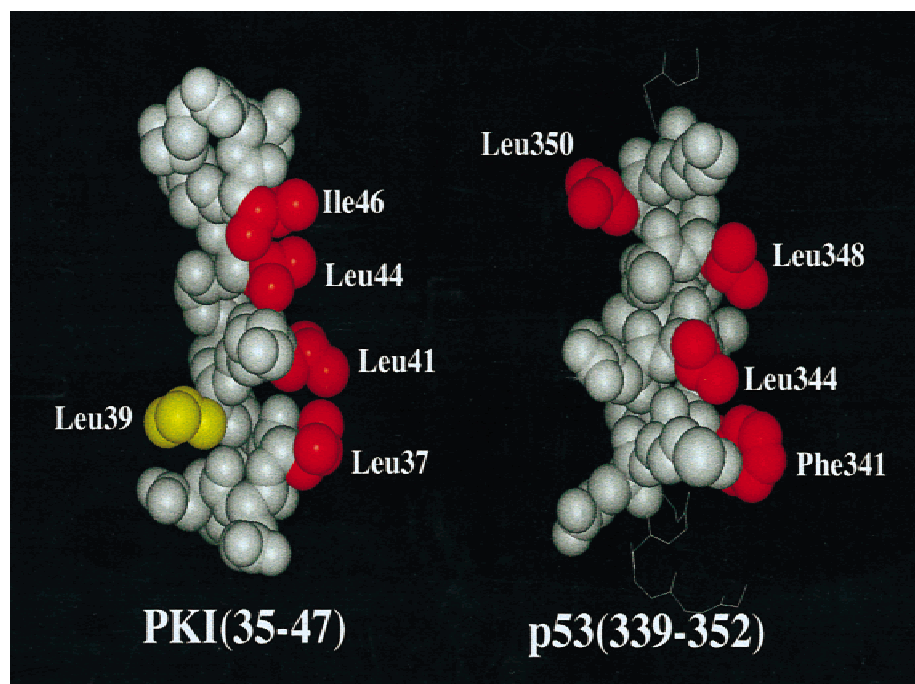


**Fig. 7.** Space filling model of PKI $\alpha$ (35–47) and p53(339–351) (IPES) (Lee et al., 1994). The essential hydrophobic residues for each nuclear export signal are labeled and shown in red. Leu39, the only hydrophobic residue in the helix not to play a role in nuclear export, is shown in yellow.

a distinct biological function. We show here that Helix I starts with the N-terminal capping box motif, Thr-Asp-Val-Glu, at the N-terminus of the protein, extends to Ser13, and is the helix responsible for high-affinity binding to the C subunit. Residues critical for this interaction have been previously determined by mutational studies (Walsh et al., 1990), and the crystal structure of the C subunit-PKI $\alpha$  (5–24) complex showed that hydrophobic residues on one face of this helix interact with a hydrophobic pocket on the surface of the C-subunit (Knighton et al., 1991b). The N-terminus of PKI $\alpha$ , which extends the helix by one full turn, is a highly conserved region among PKI isoforms, including murine PKI $\beta$ 2 in which this region is preceded by a 21 amino acid sequence. This N-terminal capping box acts to anchor the formation of this high affinity binding helix of PKI. This extension may create an additional interaction between Asp2 of PKI $\alpha$  and Arg256 of the C subunit since previous work with inhibitory peptides showed a tighter C-subunit affinity for the PKI $\alpha$ (1–24) peptide than a PKI $\alpha$ (5–24) peptide (Scott et al., 1985).

In the crystal structure, Gly14 of PKI is part of a turn from Gly14 to Gly17 followed by an extended structure of the pseudo-substrate site in a groove between the small and large lobes of the kinase (Knighton et al., 1991b). In the protein free in solution, no such turn was observed and no structural information was obtained for the five-residue consensus recognition sequence, encompassing Arg18 to Ile22. This region is much more flexible than the binding helix. A parallel NMR study of PKI peptides from the N-terminal region up to Asp24 showed that bent structures are present in solution, with the consensus recognition sequence running antiparallel to Helix I. However, such structures are highly dependent on the solution conditions, especially the pH (Padilla et al., 1997). The binding of PKI $\alpha$  to the C-subunit is bipartite with the basic consensus site docking with low affinity to the active site cleft and the N-terminal helix required for high-affinity binding. The existence of the helix free in solution followed by a flexible consensus sequence can permit high-affinity docking of PKI to the hydrophobic pocket of the C-subunit subsequent to the long-range electrostatic attraction of the positively charged consensus sequence to the negatively charged active site region of the kinase.

Helix II, from residue 35 to 44, is well defined by medium range NOE connectivities but has fraying N- and C-termini with a C-terminal half less resolved than the N-terminal half. Many of the hydrophobic residues in the 37–46 sequence are critical for the nuclear export function of PKI. As shown in Figure 7, three leucines (Leu37, Leu41, and Leu44) form a hydrophobic face to Helix II. Mutation of Leu41 and Leu44 to alanine in NES containing peptides do not affect the structural properties of the peptide (J.A. Hauer, unpubl. data) while abolishing nuclear export (Wen et al., 1995). The structure of the C-terminus of Helix II could not be determined unambiguously since NMR data for the Leu44–Asn47 segment does not correspond to a standard turn pattern (Wüthrich, 1986). In the canonical turns of type I, I', II, and III, at least one small  $J_{\alpha N}$  coupling constants is expected to occur. While the amide hydrogens in this region exhibit slow exchange in D<sub>2</sub>O, no small coupling constants (smallest at 6.3 Hz for Leu44) were observed.

A growing number of other nuclear export signals have either been proposed or identified in other proteins based on the repetition of leucine residues. These include Rev, MAPKK, and p53 (Fischer et al., 1995; Fukuda et al., 1996; Middeler et al., 1997). We show, in this work, that leucine residues in the NES motif of PKI $\alpha$  cluster within a hydrophobic surface on Helix II. The region

of p53 proposed to contain the Nuclear Export Signal (residues 341–350) is also helical and shows a similar distribution of large hydrophobic residues in an amphipathic  $\alpha$ -helix (Fig. 7; Lee et al., 1994). The formation of a highly hydrophobic surface of leucines is likely representative of such motifs since they are postulated to use common cellular machinery, the most likely binding partner being recently identified as CRM1 (Fornerod et al., 1997; Stade et al., 1997).

Another region of flexible structure occurs for residues Asp54 to Arg57. In this case, however, a small  $J_{\alpha N}$  coupling constant is observed for Ala55, and the  $d_{\alpha N}(54,56)$  has a higher intensity than that observed in the Leu44–Asn47 segment. Interestingly, slow NH exchange rates are observed for residues encompassing this region, indicating that it is not fully exposed to solvent. This further defines this region as another flexible turn structure with, as yet, no known function.

In closing, it can be concluded that PKI $\alpha$  contains two relatively stable helices, which are essential for the two functional properties of PKI $\alpha$ : high affinity binding to the C subunit and nuclear export. According to the NMR data, 22 residues are found in these two helical domains within residues 2–13 and 35–44. The presence of 22 helical residues, as inferred from our NMR data, is slightly greater than the  $\alpha$ -helical content of 21% previously reported by CD (Thomas et al., 1991). The  $\beta$ -sheet structure determined by CD was not found by NMR in the fragments of PKI $\alpha$ . This may be due to aggregation of full length PKI in solution, where  $\beta$ -sheet structures may form in the aggregates. The remainder of PKI $\alpha$  is thus remarkable for its lack of well-defined or stable secondary structure. p21 and p16, two regulatory proteins that bind to CDK2, display similar properties and are largely unstructured when they are free in solution (Kriwacki et al., 1996; Russo et al., 1996). This property may be characteristic of many of the small proteins that bind to protein kinases and regulate their function.

## Materials and methods

### Preparation of NMR samples

The [Gly0]PKI $\alpha$  cDNA corresponding to rabbit skeletal muscle with a glycine residue between the start methionine and the first residue was the gift of Dr. R.A. Maurer (Volum Institute, Portland, Oregon). This was transformed into *Escherichia coli* BL21 (DE3) and grown in minimal media with either (<sup>15</sup>NH<sub>4</sub>)<sub>2</sub>SO<sub>4</sub> or <sup>15</sup>NH<sub>4</sub>Cl as the sole nitrogen source. The protein was purified as described previously (Thomas et al., 1991). The numbering of residues throughout this work refers to the rabbit skeletal muscle protein kinase inhibitor (PKI $\alpha$ ).

The [I<sub>26</sub>M]PKI $\alpha$  vector, in a derivative of pET3C with tetracycline resistance, was graciously provided by Dr. R.A. Maurer. The protein was expressed and purified as above. The purified protein was digested with cyanogen bromide in 70% formic acid and the resulting peptides were separated by HPLC chromatography and identified with a gas phase amino acid sequencer with an on-line PHT analyzer (Applied Biosystems, Inc. models 470A and 120). Vydac C18 analytical or semi-prep columns were used. Solvent A was 0.1% TFA in MQ water, and B was 0.85% TFA in ACN/MQ water (95:5). The <sup>15</sup>N enriched PKI sample was prepared by mixing 8 mg protein in 450  $\mu$ L (2.2 mM) of solvent (D<sub>2</sub>O or a mixture of 95% H<sub>2</sub>O/5% D<sub>2</sub>O), and the pH adjusted to 6.6. Samples of [Gly<sub>0</sub>]PKI $\alpha$ (1–25) were prepared by dissolving 6.2 mg of peptide

in 450  $\mu$ L (5 mM) of solvent ( $D_2O$  or a mixture of 95%  $H_2O$ /5%  $D_2O$ ), and the pH adjusted to between 3.8 and 4.1. The PKI $\alpha$ (26–75) sample was prepared by dissolving 5.9 mg of peptide in 450  $\mu$ L (2.5 mM) of solvent ( $D_2O$  or a mixture of 95%  $H_2O$ /5%  $D_2O$ ), and adjusted to a pH of 7.1. All samples were sealed under argon.

#### Choice of experimental conditions

Preliminary homonuclear NMR studies of PKI $\alpha$  at 32 °C by DQF-COSY and jump-return NOESY techniques indicated low NOE intensities and strong signal overlap (data not shown). Chemical shift dispersion and linewidths were unaffected by increased ionic strength, up to 100 mM NaCl or 50 mM  $MgSO_4$ , or decreased protein concentration to 0.5 mM. However, decreasing the temperature had two effects: (1) the NOE intensities increased, and (2) NH exchange was slow enough to allow the use of water presaturation. Even though NH intensities were not affected by temperature changes between 2 and 12 °C, the NOEs involving NH or side-chain protons were stronger at the lower temperature.

#### NMR techniques

Spectra of  $^{15}N$  labeled-[Gly0]PKI $\alpha$  and unlabeled [Gly0]PKI $\alpha$ (1–25) and PKI $\alpha$ (26–75) were recorded at 600 MHz on an AMX 600 Bruker spectrometer. Heteronuclear experiments were carried out at 2 and 12 °C. The  $^{15}N$ - $^1H$  HSQC,  $^{15}N$ - $^1H$  HMQC-TOCSY, and  $^{15}N$ - $^1H$  HMQC-NOESY spectra were run with the published sequences (Bodenhausen & Ruben, 1980; Bax et al., 1990; Norwood et al., 1990), respectively. The HSQC was recorded with spectral widths of 1,824 and 6,613 Hz while the HMQC-TOCSY and HMQC-NOESY spectra and were recorded with spectral widths of 1,946 and 6,024 Hz in the  $^{15}N$  and  $^1H$  dimensions, respectively. For each 2D experiment, 2,048 points by 512 FIDs (128 for the HSQC) were recorded. Water suppression was achieved with 1s presaturation. Eighty scans were collected for the HMQC-NOESY with 150 and 200 ms mixing times, and 32 scans were collected with a mixing time of 48 ms for the HMQC-TOCSY experiments. TPPI was used in t1 for all experiments (Marion & Wüthrich, 1983).

Homonuclear experiments on the PKI fragments were carried out at 2 °C. The NOESY, TOCSY, and DQF-COSY spectra were recorded with a spectral width of 6,024 Hz, with 1s water presaturation. For each 2D experiment, 4,096 data points by 512 FIDs were recorded. Eighty scans were run for both the NOESY (with a 200 ms mixing time) and the TOCSY (with 40 ms mixing time) experiments, and 128 scans for the DQF-COSY.

Slow exchanging amide protons were determined for each fragment by recording two 30 min COSY experiments at 2 °C just after dissolving the peptides in  $D_2O$ . The data collected were 2,048 points by 512 FIDs.

After Fourier transform, data sets of 2,048 by 512 real points were further processed by polynomial baseline correction in both dimensions. Coupling constants between CaH and NH were measured from the DQF-COSY experiments after reprocessing the data with 0.3 Hz per point resolution in the F2 dimension. The  $^1H$ -NMR chemical shifts at 2 °C were referenced by taking water resonance at 5.14 ppm referenced against  $tspd_4$ . All  $^{15}N$ -NMR chemical shifts were referenced according to external 1.85 M  $^{15}NH_4Cl$  in 1 M HCl at 24.93 ppm.

#### Chemical Shift Index analysis

The CaH chemical shifts of  $^{15}N$ [Gly0]PKI $\alpha$  were analyzed by the Chemical Shift Index (Wishart et al., 1992). Briefly, the measured CaH chemical shift values in ppm were subtracted from the tabulated values for each residue. If the difference was greater than 0.1 ppm, a value of +1 was assigned to the residue. If the difference was more negative than -0.1 ppm, a value of -1 was assigned. A value of 0 was assigned to all other residues. A local density of three or more +1 indices over 70% of the residues in a stretch is indicative of a  $\beta$ -strand, and a local density of 4 or more -1 indices over 70% of the residues in a stretch is indicative of an  $\alpha$ -helix. Termination of secondary structures can be identified by a chemical shift index of the opposite sign or by two consecutive zeros.

#### Experimental constraints

NOE constraints were derived from the NOESY spectra at 200 ms mixing time and applied as 3.0, 4.0, and 4.7 Å upper limits for strong, medium, and weak NOEs, respectively. Pseudo-atom corrections were added (Wüthrich et al., 1983). Distance constraints for hydrogen bonds were not introduced. Values of  $J\alpha N$  coupling constants listed in Figure 2 were directly used in the final refinement stage.

#### Computer modeling methods

Modeling of [Gly0]PKI $\alpha$ (1–25) and the peptide stretch Ser34–Lys48 of PKI $\alpha$ (26–75) was performed by distance geometry and simulated annealing using the X-PLOR program Version 3.8 (Brünger, 1992) on an HP 735 work station and is based on the original work of Clore and Gronenborn and others (Nilges et al., 1988a, 1988b). Distance geometry was applied to a subset of atoms (Ca, Ha, N, NH, C, C $\beta$ , and C $\gamma$ ) to generate 30 substructures. Simulated annealing was done by 3 ps molecular dynamics at 2,000 K (where the force constants were increased in small steps), an annealing step consisting of 5 ps dynamics during which the temperature was decreased from 2,000 to 100 K in 50 K steps, and 200 cycles of Powell minimization with constraints. The refinement protocol consisted of 10 ps dynamics during which the temperature was decreased from 1,000 to 100 K in 50 K steps and 200 cycles of Powell minimization with constraints. The structures were further refined by applying 200 cycles of Powell minimization and 20 ps dynamics at 300 K, where an electrostatic energy term was introduced. Finally, direct J-coupling refinement was done by applying 5,000 cycles of Powell minimization introducing a  $J\alpha N$ -coupling error term (Kuszewski et al., 1995). Structures were selected using the following criteria: (1) no violation of distance constraints greater than 0.5 Å, and (2) good geometry (ca. RMSD from ideality for bonds or angles less than 0.01 Å or 2°, respectively). An average structure was obtained by fitting backbone atoms from residue 1 to 13 for [Gly0]PKI $\alpha$ (1–25) and from residue 35 to 44 for PKI $\alpha$ (26–75). The average RMSD value for the superimposition of these backbone stretches was 1.11 and 1.30 Å, respectively. Both average structures were further minimized by applying 1,000 cycles of Powell minimization.

#### Ensemble-averaged refinement

The protocol used is similar to the one described by Bonvin and Brünger (1995), starting from the averaged structures of

[Gly0]PKI $\alpha$ (1–25) and PKI $\alpha$ (26–75). Briefly, cross validation (Brünger et al., 1993) was performed on the NOE data alone (Bonvin & Brünger, 1995). Cross-validated RMSDs from the experimental distance restraints and the number of violations  $>0.2$  Å as a function of the number of conformers were used for assessing the validity of multiconformer refinement and thus to avoid over-fitting. In both [Gly0]PKI $\alpha$ (1–25) and PKI $\alpha$ (26–75), single conformer refinement gave the most accurate representation of the structure.

The ensemble of conformers was obtained by generating multiple identical copies of the initial structure (Bonvin & Brünger, 1995). The NOE distance restraints were introduced with ensemble-averaging using a square-well restraining potential, and  $W_{\text{NOE}}$  was set to 50 kcal mol $^{-1}$  Å $^{-2}$ . A  $J\alpha N$  coupling potential (Kuszewski et al., 1995) was included and no ensemble-averaging was applied for these additional restraints. A simulated annealing protocol consisting of 5 ps constant temperature dynamics at 1,000 K followed by a slow-cooling annealing from 1,000 to 1 K was used for refinement. Finally, the structures were subjected to 200 steps of conjugate gradient minimization. An average structure obtained in this way may contain unrealistic, strained geometry and give a poor representation of the ensemble. To avoid this, the method proposed by DeLano and Brünger (1994) based on a three-dimensional probability map refinement was used (DeLano & Brünger, 1994). The probability map was computed by superimposing the structures on the average C $\alpha$  coordinates and defining a three-dimensional map enclosing these structures. Then, the same refinement protocol as described by DeLano and Brünger (1994) was used in X-PLOR (200 steps of minimization, slow-cooling annealing from 3,000 to 300 K over 2.7 ps, followed by 120 steps of energy minimization without NMR restraints but with probability map restraints), with, in addition, a slow-cooling annealing from 1,000 to 1 K in 1 ps including NMR (distance and J-coupling) restraints.

### Supplementary material in Electronic Appendix

Table 1. Chemical shift assignments for PKI $\alpha$  and the two PKI $\alpha$  peptides at 2 °C (file name NMR assignments). Nitrogen chemical shifts were referenced to external  $^{15}\text{NH}_4\text{Cl}$  (1.85 M) in 1 M HCl at 24.93 ppm relative to liquid ammonia and proton chemical shifts were referenced to the  $^1\text{H}_2\text{O}$  signal at 5.14 ppm. (A) Chemical shift assignments for  $^{15}\text{N}$  labeled PKI $\alpha$  at pH 6.6. (B)  $^1\text{H}$  chemical shift assignments for [Gly0]PKI(1–25) at pH 4.1. (C)  $^1\text{H}$  chemical shift assignments for PKI $\alpha$ (26–75) at pH 7.1.

### Acknowledgments

This work was supported by funding from the University of California Tobacco-Related Disease Research Program (2RT0066) to SST and the PICS (141 CNRS-MAE, France) to JP. JAH is a Fellow of the Markey Charitable Trust. We thank Dr. Richard Maurer for generously providing the PKI $\alpha$  expression vectors and Siv Garrod for purifying the peptides.

### References

Ashby CD, Walsh DA. 1973. Characterization of the interaction of a protein inhibitor with adenosine 3'-5'-monophosphate-dependent protein kinases. *J Biol Chem* 248:1255–1261.

Bax A, Ikura M, Kay LE, Torchia DA, Tschudin R. 1990. Comparison of different modes of two-dimensional reverse-correlation NMR for the study of proteins. *J Magn Res* 86:304–318.

Bodenhausen G, Ruben DJ. 1980. Natural abundance nitrogen-15 NMR by enhanced heteronuclear spectroscopy. *Chem Phys Lett* 69:185–189.

Bonvin AMJ, Brünger AT. 1995. Conformational variability of solution nuclear magnetic resonance structures. *J Mol Biol* 250:80–93.

Brünger AT. 1992. *X-PLOR: A system for X-ray crystallography and NMR*. New Haven, Connecticut: Yale University.

Brünger AT, Clore MG, Gronenborn AM, Saffrich R, Nilges M. 1993. Assessing the quality of solution nuclear magnetic resonance structures by complete cross-validation. *Science* 261:328–331.

DeLano WL, Brünger AT. 1994. Helix packing in proteins: Prediction and energetic analysis of dimeric, trimeric and tetrameric GCN4 coiled coil structures. *Proteins Struct Funct Genet* 20:105–123.

Dell'Acqua M, Scott JD. 1997. Protein kinase A anchoring. *J Biol Chem* 272:12881–12884.

Fantozzi DA, Harootyan AT, Wen W, Taylor SS, Feramisco JR, Tsien RY, Meinkoth JL. 1994. Thermostable inhibitor of the cAMP-dependent protein kinase enhances the rate of export of the kinase catalytic subunit from the nucleus. *J Biol Chem* 269:2676–2686.

Fischer U, Huber J, Boelens WC, Mattaj JW, Luhrmann R. 1995. The HIV-1 Rev activation domain is a nuclear export signal that accesses an export pathway used by specific cellular RNAs. *Cell* 82:475–483.

Fornerod M, Ohno M, Yoshida M, Mattaj JW. 1997. CRM1 is an export receptor for leucine-rich nuclear export signals. *Cell* 90:1051–1060.

Fukuda M, Gotoh I, Gotoh Y, Nishida E. 1996. Cytoplasmic localization of mitogen-activated protein kinase kinase directed by its NH2-terminal, leucine-rich short amino acid sequence, which acts as a nuclear export signal. *J Biol Chem* 271(33):20024–20028.

Knighton DR, Zheng J, Ten Eyck LF, Ashford VA, Xuong N-H, Taylor SS, Sowadski JM. 1991a. Crystal structure of the catalytic subunit of cAMP-dependent protein kinase. *Science* 253:407–414.

Knighton DR, Zheng J, Ten Eyck LF, Xuong N-H, Taylor SS, Sowadski JM. 1991b. Structure of a peptide inhibitor bound to the catalytic subunit of cyclic adenosine monophosphate-dependent protein kinase. *Science* 253:414–420.

Kriwacki RW, Hengst L, Tennant L, Reed SI, Wright PE. 1996. Structural studies of p21 Waf1/Cip1/Sdi1 in the free and Cdk2-bound state: Conformational disorder mediates binding diversity. *Proc Natl Acad Sci USA* 93:11504–11509.

Kuszewski J, Gronenborn AM, Clore GM. 1995. The impact of direct refinement against proton chemical shifts on protein structure determination by NMR. *J Magn Res Series B* 107(3):293–297.

Lee W, Harvey T, Yin Y, Yau P, Litchfield D, Arrowsmith CH. 1994. Solution structure of the tetrameric minimum transforming domain of p53. *Nature Struct Biol* 1:877–890.

Ludvigsen S, Andersen KV, Poulsen FM. 1991. Accurate measurements of coupling constants from two-dimensional NMR spectra of proteins and determination of phi-angles. *J Mol Biol* 217:731–736.

Marion D, Wüthrich K. 1983. Application of phase-sensitive two-dimensional correlated spectroscopy (COSY) for measurements of  $^1\text{H}$ - $^1\text{H}$  spin-spin coupling constants in proteins. *Biochem Biophys Res Commun* 113:967–974.

Merutka G, Dyson HJ, Wright PE. 1995. "Random coil"  $^1\text{H}$  chemical shifts obtained as a function of temperature and trifluoroethanol concentration for the peptide series GGXGG. *J Biomol NMR* 5:14–24.

Middleer G, Aerf K, Jenovai S, Thulig A, Tschodrich-Rotter M, Kubitschek U, Peters R. 1997. The tumor suppressor p53 is subject to both nuclear import and export, and both are fast, energy-dependent and lectin-inhibited. *Oncogene* 14:1407–1417.

Nilges M, Clore GM, Gronenborn AM. 1988a. Determination of three-dimensional structures of proteins from interproton distance data by dynamical simulated annealing from a random array of atoms. *FEBS Lett* 239:129–136.

Nilges M, Clore GM, Gronenborn AM. 1988b. Determination of three-dimensional structures of proteins from interproton distance data by hybrid distance geometry-dynamical simulated annealing calculations. *FEBS Lett* 239:317–324.

Norwood TJ, Boyd J, Heritage JE, Soffe N, Campbell ID. 1990. Comparison of techniques for  $^1\text{H}$ -detected heteronuclear  $^1\text{H}$ - $^{15}\text{N}$  spectroscopy. *J Magn Reson* 87:488–501.

Padilla A, Hauer J, Tsigelny I, Parello J, Taylor S. 1997. Solution structure of synthetic peptide inhibitor and substrate of cAMP-dependent protein kinase: A study by 2D  $^1\text{H}$  NMR and molecular dynamics. *J Pept Res* 49:210–220.

Presta LG, Rose GD. 1988. Helix signals in proteins. *Science* 240:1632–1641.

Reed J, de Ropp JS, Trewhella J, Glass DB, Liddle WK, Bradbury EM, Kinzel V, Walsh DA. 1989. Conformational analysis of PKI(5–22) amide, the active inhibitory fragment of the inhibitor protein of the cyclic AMP-dependent protein kinase. *Biochem J* 264:371–380.

Richardson JS, Richardson DC. 1988. Amino acid preferences for specific locations at the ends of alpha-helices. *Science* 240:1648–1652.

- Russo AA, Jeffrey PD, Patten AK, Massague J, Pavletich NP. 1996. Crystal structure of the p27Kip1 cyclin-dependent-kinase inhibitor bound to the cyclin A-CDK2 complex. *Nature* 382:325–331.
- Scott JD, Fischer EH, Demaille JG, Krebs EG. 1985. Identification of an inhibitory region of the heat-stable protein inhibitor of the cAMP-dependent protein kinase. *Proc Natl Acad Sci USA* 82:4379–4383.
- Stade K, Ford CS, Guthrie C, Weis K. 1997. Exportin 1 (Crm1p) is an essential nuclear export factor. *Cell* 90:1041–1050.
- Taylor SS, Buechler JA, Yonemoto W. 1990. cAMP-dependent protein kinase: Framework for a diverse family of regulatory enzymes. *Ann Rev Biochem* 59:971–1005.
- Thomas J, Van Patten SM, Howard P, Day KH, Mitchell RD, Sosnick T, Trehwella J, Walsh DA, Maurer RA. 1991. Expression in *Escherichia coli* and characterization of the heat-stable inhibitor of the cAMP-dependent protein kinase. *J Biol Chem* 266:10906–10911.
- Walsh DA, Angelos KL, Van Patten SM, Glass DB, Garetto LP. 1990. The inhibitor protein of the cAMP-dependent protein kinase. In: Kemp BE, ed. *Peptides and protein phosphorylation*. Boca Raton: CRC Press, Inc. pp 43–84.
- Walsh DA, Ashby CD, Gonzalez C, Calkins D, Fischer EH, Krebs EG. 1971. Purification and characterization of a protein inhibitor of adenosine 3',5'-monophosphate-dependent protein kinases. *J Biol Chem* 246:1977–1985.
- Wen W, Meinkoth JL, Tsien RY, Taylor SS. 1995. Identification of a signal for rapid export of proteins from the nucleus. *Cell* 82:463–473.
- Whitehouse S, Walsh DA. 1982. Purification of a physiological form of the inhibitor protein of the cAMP-dependent protein kinase. *J Biol Chem* 257: 6028–6032.
- Wishart D, Sykes B, Richards F. 1992. The Chemical Shift Index: A fast and simple method for the assignment of protein secondary structure through NMR spectroscopy. *Biochemistry* 31(6):1647–1651.
- Wüthrich K. 1986. *NMR of proteins and nucleic acids*. New York: John Wiley & Sons.
- Wüthrich K, Billeter M, Braun W. 1983. Pseudo-structures for the 20 common amino acids for use in studies of protein conformation by measurements of intramolecular proton-proton distance constraints with nuclear magnetic resonance. *J Mol Biol* 169:949–961.
- Zheng JH, Knighton DR, Parello J, Taylor SS, Sowadski JM. 1991. Crystallization of the catalytic subunit of cyclic adenosine monophosphate-dependent protein kinase. *Methods Enzymol* 200:508–521.
- Zhou H, Lyu P, Wemmer D, Kallenbach N. 1994. Alpha helix capping in synthetic model peptides by reciprocal side chain-main chain interactions: Evidence for an N-terminal "capping box." *Proteins* 18(1):1–7.